CHAPTER 15

Photocatalytic Reactor Design

JAVIER MARUGÁN*[a], RAFAEL VAN GRIEKEN[a], ALBERTO E. CASSANO[†b], AND ORLANDO M. ALFANO[b]

[a]Universidad Rey Juan Carlos, C/Tulipán s/n, 28933 Móstoles, Spain; [b]INTEC, UNL-CONICET, Ruta Nacional N° 168, 3000 Santa Fe, Argentina
*E-mail: javier.marugan@urjc.es

15.1 Predictive Design of Photocatalytic Reactors

The simulation and full predictive design of large-scale photocatalytic reactors can be carried out by solving the conservation equations of momentum, energy and mass on the system, similarly to conventional chemical reactors. The momentum and mass balance equations take the same expressions as those corresponding to thermal reactors, as they depend on the fluid dynamic behavior of the reactor (well-mixed, plug-flow, axial dispersion, *etc.*), the relevant mass transfer mechanism (diffusion and/or convection) and the expression corresponding to the reaction rate taking into consideration the stoichiometry of the chemical reactions. In contrast, the classic enthalpy balance that describes the heat flows and temperature profiles in thermal chemical reactors is substituted in photochemical reactors by the radiative energy balance. The reason for this is that reactions are photochemically and not thermally activated. Consequently, the temperature profiles and thermal effects on the chemical reaction step can usually be neglected, although they

[†]Deceased 12 July 2014.

RSC Energy and Environment Series No. 14
Photocatalysis: Fundamentals and Perspectives
Edited by Jenny Schneider, Detlef Bahnemann, Jinhua Ye, Gianluca Li Puma, and Dionysios D. Dionysiou

Published by the Royal Society of Chemistry, www.rsc.org

can be relevant in some of the physical processes coupled to the reaction, such as mass transfer and adsorption. On the other hand, resolution of the radiation transfer equation (RTE) becomes critical for the simulation of photocatalytic reactors.

To solve the mass balance of the reactor, a kinetic model should be introduced in the expression of the reaction rate. Typically, this kinetic model expression is determined at laboratory scale under well-defined and controlled conditions. In photocatalytic processes, this requirement is even more important, as it also means that the radiation profile in the kinetic laboratory reactor should be perfectly known.

The necessity of radiation absorption to trigger the chemical reaction means that conventional kinetic equations are useless, as they require the use of intrinsic kinetic models that take into account the rate of photon absorption in an explicit way. Only an intrinsic kinetic model based on the reaction mechanism and describing explicitly the effect of the radiation absorption could be used for predictive simulation of photoreactor design and geometries different from that in which the model parameters have been calculated.

Figure 15.1 schematizes the methodology for the predictive simulation of large-scale photocatalytic reactors based on the determination of the kinetics at laboratory scale. The estimation of the kinetic parameters of the proposed mechanistic model is based on the minimization of the error between the predictions of the model for the evolution of the concentration of the species along time ($C_i^{\mathrm{CALC}}(t)$) and the experimental data ($C_i^{\mathrm{EXP}}(t)$). The predictions are generated by solving the mass balances of the laboratory reactor, ideally behaving close to well-mixed conditions for the aim of simplicity, or

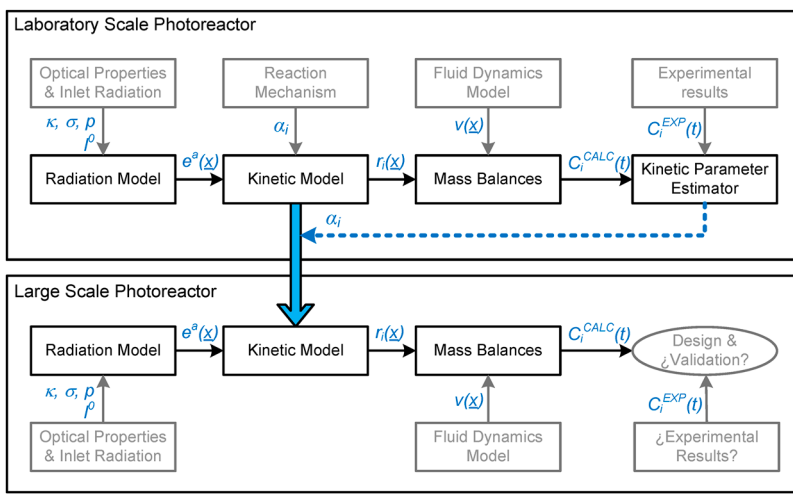

Figure 15.1 Schematic flowchart of the methodology for the predictive simulation of photocatalytic reactors based on the determination of the intrinsic kinetics at laboratory scale.

considering the reactor velocity field ($v(\underline{x})$). Calculation of the reaction rate at any position of the reactor ($r(\underline{x})$) requires that the kinetic model expression include the effect of the local volumetric rate of photon absorption ($e^a(\underline{x})$), which will be markedly different along the reactor due to the unavoidable radiation profiles. The values of the $e^a(\underline{x})$ have to be computed through the resolution of the radiation model of the reactor, which would consider not only the geometry and the boundary conditions corresponding to the power and spectrum of the radiation source (I^0) but also the optical properties of the photocatalytically active material inside the reactor (κ,σ,p). These optical properties have been reported in the literature for common TiO_2 materials such as P25 TiO_2,[1] but their determination is critical for reactor designs based on new developed photocatalysts.[2]

Once the intrinsic kinetics of the process have been determined at laboratory scale, the full predictive simulation of a large-scale photocatalytic reactor can be addressed by following the same procedure of sequential resolution of the radiation model, kinetic model and mass balance of the system, but considering in this case the geometry, irradiation source and fluid dynamic model corresponding to the designed reactor. The details of this procedure will be described in the next sections of this chapter.

15.2 Optical Properties of Photocatalytic Suspensions and Films

As described in Section 15.1, resolution of the *radiative transfer equation* (RTE) requires information about the optical properties of the photocatalytic medium:

- The spectral volumetric absorption coefficient, κ_λ, which represents the amount of radiation that is absorbed per unit length along the radiation pathway.
- The spectral volumetric scattering coefficient, σ_λ, which represents the amount of the radiation that is scattered in all directions per unit length along the radiation pathway.
- The phase function, $p_\lambda(\boldsymbol{\Omega}' \rightarrow \boldsymbol{\Omega})$, a normalized function of probabilities that describes the directional distribution of the scattered radiation. Satuf *et al.*[1] proposed the use of the Henyey–Greenstein phase function ($p_{\text{H-G},\lambda}$) as an optimal choice for the description of complex multiple scattering phenomena in photocatalytic systems using a single parameter. This function is given by:

$$p_{\text{H-G},\lambda}(\mu_0) = \frac{\left(1 - g_\lambda^2\right)}{\left(1 + g_\lambda^2 - 2g_\lambda\mu_0\right)^{3/2}} \tag{15.1}$$

where g_λ is the so-called *asymmetry factor*. The main feature of this equation is that one parameter is able to represent very different behaviors, from simple

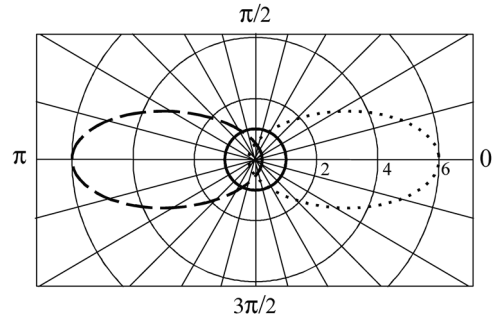

Figure 15.2 Distribution of probabilities of scattering as a function of the angle according to the Henyey–Greenstein phase function for different values of g_λ: solid line, $g_\lambda = 0.0$; dashed line, $g_\lambda = -0.5$; dotted line, $g_\lambda = 0.5$. (Reprinted with permission from ref. 1. Copyright 2005 American Chemical Society.)

isotropic scattering ($g = 0$, $p_\lambda = 1$) to different shapes of scattering predominantly forward ($g > 0$) or backwards ($g < 0$), as represented in Figure 15.2.

The values of the optical properties of the photocatalytic medium strongly depend on a number of physical and operation variables. Among them, the chemical composition of the photocatalytic material, including the type of semiconductor (TiO_2, ZnO, *etc.*), presence of dopants, surface modifications, and other variables that modify the intrinsic absorption spectra of the solid material. The physical arrangement of the material in the reactor is also critical. For instance the optical properties of a photocatalytic coating depend on the porosity and other physical properties of the film. Regarding the use of particle suspensions, the optical properties are significantly modified by the size of the agglomerates, which is strongly conditioned not only by the size of the primary particles but also by the degree of agglomeration, which depends on the mixing conditions, the pH (as it modifies the surface charge of the particles, especially near the zero point charge value), and the chemical composition of the solution. As a consequence, rigorous estimation of the radiation absorbed by the system requires prior determination of the optical properties under the experimental conditions in which the reactor will be operating, including their possible variation during the reaction, for instance owing to changes in the pH of the disappearance (or appearance) of absorbing chemical species.

The experimental determination of the optical properties of newly developed materials can be carried out with relatively simple spectrophotometric measurements. For particulate materials in suspension, a flow cell should be used to avoid settlement and to reproduce as closely as possible in the reservoir tank the agglomeration of particles under the reaction conditions.[2] First of all, the spectral values of the extinction coefficient (the sum of the absorption and scattering coefficient according to eqn 14.16, Chapter 14) can be directly estimated from conventional transmittance measurements, using a slit with a small hole to make sure that all photons that have changed of direction are discarded (Figure 15.3).

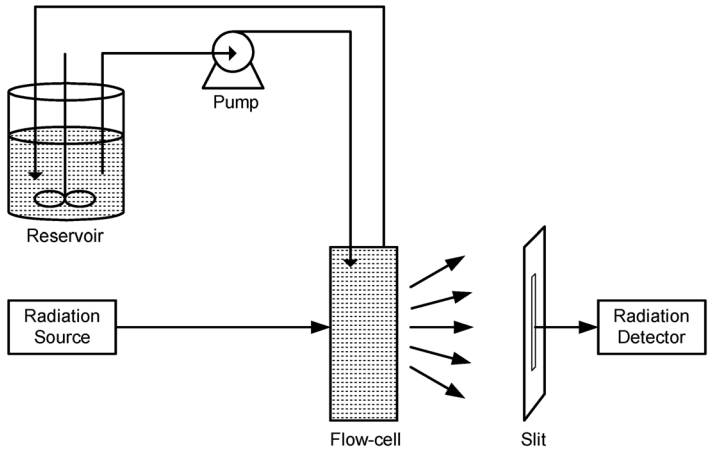

Figure 15.3 Experimental setup for measurement of the suspension transmittance. (Reprinted from ref. 2. Copyright 2006 American Institute of Chemical Engineers, with permission from John Wiley & Sons.)

The Napierian volumetric extinction coefficient (β_λ) is calculated from the transmittance readings at each wavelength, T_λ, as follows:

$$\beta_\lambda(\mathrm{cm}^{-1}) = \frac{-\ln(T_\lambda)}{L(\mathrm{cm})} \tag{15.2}$$

where L represents the cell path length. By repeating these measurements for different material loadings, the specific extinction coefficient, β_λ^* ($\mathrm{cm}^2\ \mathrm{g}^{-1}$), can be obtained by application of a standard linear regression on the data with forced intercept at the origin, providing a way to estimate the value of this optical property at untested catalyst loadings.

Evaluation of the absorption coefficient and the asymmetry factor of the Henyey–Greenstein phase function requires two additional independent measurements, these being the scattering coefficient calculation by subtraction from the extinction coefficient. These additional experiments consist of diffuse transmittance (DT_λ) and diffuse reflectance (DR_λ) spectrophotometric measurements carefully designed to collect all the radiation scattered by the sample by means of an integrating sphere (Figures 15.4 and 15.5, respectively).

The radiation scattered through both sides of the cell is lost and not accounted for by the detector; consequently, the absorption coefficient and phase function cannot be directly calculated from these measurements. However, the resolution of RTE inside the spectrophotometric cell can provide the theoretical values of DT_λ and DR_λ given by:

$$\mathrm{DT}_\lambda = \frac{\left\langle q_\lambda^+ \right\rangle_y (x = L)}{\left\langle q_\lambda^+ \right\rangle_y (x = 0)} \tag{15.3}$$

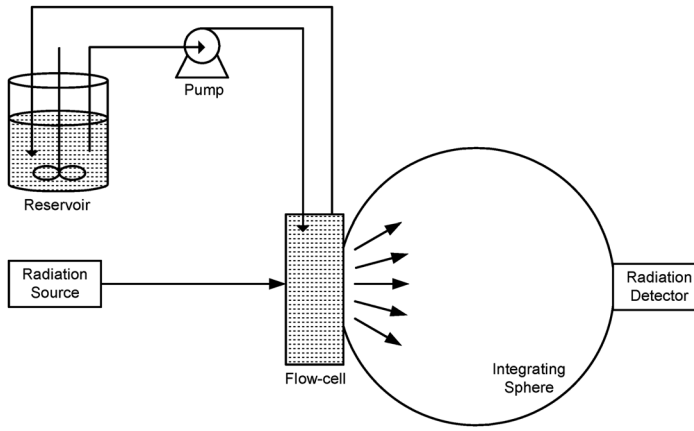

Figure 15.4 Experimental setup for measurement of the diffuse transmittance. (Reprinted from ref. 2. Copyright 2006 American Institute of Chemical Engineers, with permission from John Wiley and Sons.)

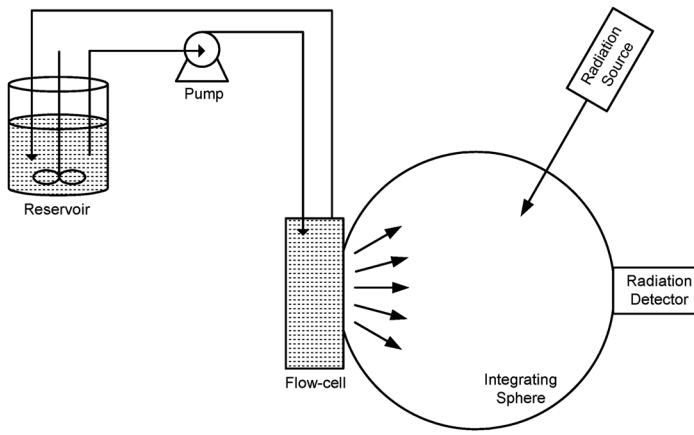

Figure 15.5 Experimental setup for measurement of the diffuse reflectance. (Reprinted from ref. 2. Copyright 2006 American Institute of Chemical Engineers, with permission from John Wiley & Sons.)

$$\mathrm{DR}_{\lambda} = \frac{\left\langle q_{\lambda}^{-} \right\rangle_{y}(x=0)}{\left\langle q_{\lambda}^{+} \right\rangle_{y}(x=0)} \tag{15.4}$$

where q^{+} and q^{-} represent the calculated radiation fluxes in the forward and backward direction, respectively. Using this data, a Levenberg–Marquardt nonlinear multiparameter estimator algorithm can be used to estimate the best values of the absorption coefficient and the asymmetry factor that minimize the errors between the experimental results and the model predictions.

Finally, experiments at different catalyst loadings would provide the information for calculation of the specific absorption coefficient, κ_λ^*.

15.3 Radiation Field Inside the Reactor

Once the optical properties of the photocatalytic medium are known, the RTE can be solved to calculate the radiation field inside a geometrically well-defined photoreaction domain, thus allowing estimation of the required local volumetric rate of photon absorption (LVRPA, Section 14.2.3) or local surface rate of photon absorption (LSRPA, Section 14.2.5) at any position of the system. The calculation of the radiation field means that the intensity of radiation (I_λ) at any position of the reactor, for every direction and for every wavelength, has to be computed. Therefore, we require the spatial, directional and spectral discretization of the RTE and consequently of the boundary conditions that define the radiation entering the reaction domain through its geometric boundaries. In addition, if the boundary condition is time-dependent (for instance when using solar light) or the optical properties of the medium change along the reaction time, time discretization of the RTE should also be carried out. More information on the different models applicable to the boundary conditions and of the RTE resolution methods can be found in Sections 14.4 and 14.5, respectively.

Once the radiation field is known, the integration of values to all directions of space gives the spectral incident radiation at any position of the system, that multiplied by the absorption coefficient at this wavelength would lead to the estimation of the monochromatic LVRPA (or LSRPA) in this spatial element. Integration of the RPA values to the whole wavelength range in which the available radiation overlaps with the absorption spectra of the photocatalytic medium would lead to the integrated LVRPA (or LSRPA) in this specific spectral range. Finally, integration of the RPA values along the spatial photoreaction domain would give the volume (or surface) average values of the photon absorption in the reactor, which are useful for computing global efficiencies of the process.

15.4 Photocatalytic Efficiencies

15.4.1 Quantum Yield and Quantum Efficiency

According to the IUPAC recommendations[3] the *quantum yield* of a photocatalytic process is defined as the ratio between the number of useful reaction events induced by the catalyst and the number of absorbed photons of a specific wavelength. This concept gives an idea of the catalyst's efficiency in the use of the absorbed photons and is usually calculated as the ratio between the reaction rate of the catalyzed chemical reaction and the rate of photon absorption. The reaction rate can be easily determined experimentally following the disappearance of the reactant or the generation of a product formed

with total selectivity. In contrast, the absorption of photons in the heterogeneous photocatalytic suspension cannot be directly measured, because the radiation extinction also includes the losses of radiation by scattering outside the reactor. Therefore, resolution of the photon balance through the RTE is required for a rigorous estimation of the amount of photons that are really absorbed in the system. As the absorption of photons (and therefore the reaction rate) is unavoidably different depending on the position inside the reactor, values averaged in the whole reactor volume should be used to be compared with the macroscopic value of the chemical reaction rate experimentally measured. With these considerations, the quantum yield of the photocatalytic reaction can be expressed as:

$$\Phi_{\lambda} = \frac{\langle r \rangle_{V_{\text{reactor}}}}{\langle e_{\lambda}^{a} \rangle_{V_{\text{reactor}}}} \tag{15.5}$$

When polychromatic radiation is used, the corresponding wavelength averaged values would be used, leading in this case to the following definition of the *quantum efficiency* (the term quantum yield is recommended to be applied only for monochromatic light):[3]

$$\eta = \langle \Phi \rangle_{\lambda} = \frac{\langle r \rangle_{V_{\text{reactor}}}}{\langle e^{a} \rangle_{V_{\text{reactor}}}} \tag{15.6}$$

Reported values for the quantum efficiencies are usually below 10%,[4] meaning that less than one tenth of the absorbed photons are used in the reaction of interest, whereas the rest of them are dissipated as heat after recombination of the generated charges.

15.4.2 Photonic Yield and Photonic Efficiency

The photonic efficiency is defined as the efficiency in the use of the photons of a photocatalytic process with respect to the total amount of photons incident to the system, and not to only those that have been absorbed:[5]

$$\xi = \frac{\langle r \rangle_{V_{\text{reactor}}} V_{\text{reactor}}}{q^{0} A_{\text{irr}}} \tag{15.7}$$

where $q^0 A_{\text{irr}}$ is the product of incident radiation flux and the irradiated surface area. This parameter, also called in the literature the *apparent quantum yield*, represents a lower limit of the true quantum yield of the process, as not all the radiation incident to the reactor will be absorbed by the catalysts. The advantage of this definition is that the incident irradiation can be easily measured experimentally by actinometric or radiometric procedures. Moreover, it gives an idea of the global efficiency of the process, because it integrates not only the efficiency of the catalytic reaction (that would be the quantum

yield) but also the efficiency of the photocatalytic material in absorbing the available light (that depends not only on its optical properties but also on the catalyst concentration) and the efficiency of the reactor design in optimizing the distribution of light for maximum absorption. Summarizing, the photonic efficiency includes the effect of design and operation variables such as the reactor geometry or the catalysts loading, whereas the quantum yield is an intrinsic value of the photocatalytic activity of the semiconductor material. When monochromatic light is employed, the photonic efficiency is referred as the *photonic yield*.[3]

15.5 Kinetic Modeling

The mechanical application of pseudo-first order and Langmuir–Hinshelwood kinetic equations usually found in the literature for the estimation of kinetic parameters of photocatalytic processes is absolutely useless for reactor design purposes. This is because the theoretical assumptions behind them are not really applicable to photocatalytic processes, as shown by several authors.[6,7] Moreover, as the process is activated by light absorption, the most important challenge concerning the modeling of the photocatalytic reaction kinetics is the determination of the influence of the photon absorption rate on the reaction rate.

In contrast with thermal reactors in which isothermal conditions can be easily achieved, unavoidable radiation profiles are always present in photocatalytic reactors. This means that a non-uniform distribution of reaction rate values would be present, and therefore the use of equations that correlate the measured macroscopic reaction rate with the incident photon flux are only valid for the experimental setup in which they have been developed. Therefore, the general engineering procedure for the simulation and design of photocatalytic reactors requires the rigorous description of the reaction rate of photocatalytic processes using intrinsic kinetic models based on the description of the reaction mechanism, in particular including the radiation activated steps.[8,9]

A general mechanism of the photocatalytic oxidation of an organic compound mediated by hydroxyl radicals should include at least the reactions corresponding to the activation of the catalyst by photon absorption, the recombination of charges, the electron and hole trapping steps and the hydroxyl radical attack on the organic compound (Table 15.1). Additionally, it should consider any other reaction relevant for the specific mechanism, such as the formation and disappearance of organic intermediates formed in the process that can compete for the hydroxyl radicals, propagation and termination steps involving reactive oxygen species and the organic compounds, direct hole transfer to the organics, adsorption of organics on, for example, the TiO_2 surface, *etc.*

Following typical assumptions in kinetic modeling such as kinetic micro steady state approximation for the unstable species (electrons, holes, radicals, *etc.*), adsorption equilibrium, constant concentration of water and

Table 15.1 Critical steps in the mechanism of the photocatalytic oxidation of an organic compound (**A**) mediated by hydroxyl radicals.

Step	Reaction	Rate
Activation	$TiO_2 + h\nu \rightarrow TiO_2 + e^- + h^+$	ϕe^a
Recombination	$e^- + h^+ \rightarrow$ heat	$k_2[e^-][h^+]$
Electron trapping	$e^- + O_2 \rightarrow {}^{\bullet}O_2^-$	$k_3[e^-][O_2]$
Hole trapping	$H_2O + h^+ \rightarrow HO^{\bullet} + H^+$	$k_4[h^+][H_2O]$
Hydroxyl attack	$\mathbf{A} + HO^{\bullet} \rightarrow$ —	$k_5[{}^{\bullet}OH][A]$
Propagation	—	
Termination	—	

oxygen, *etc.*, the expression of the disappearance rate of the organic species A could be derived. In general, the expression takes the form of:

$$r_A = -\alpha_1 f(C_i) g(e^a) \tag{15.8}$$

where α_1 is a kinetic parameter that integrates some of the kinetic constants and concentrations of species that can be assumed to remain constant, $f(C_i)$ is a general function that establishes the dependence of the reaction rate on the concentration of the organic species (reactant and intermediates) and $g(e^a)$ is a general function that describes the dependence on the rate of photon absorption. The exact form for the functions $f(C_i)$ and $g(e^a)$ will depend on each case. For instance, in a very ideal situation in which both the dependence on the concentration of *A* and the rate of photon absorption are linear it would take the form:

$$r_A = -\alpha[A]e^a \tag{15.9}$$

In other cases, the expression could be similar to:

$$r_A = -\alpha_1 \frac{[A]}{1 + \alpha_2[A]}\left(-1 + \sqrt{1 + \alpha_3 e^a}\right) \tag{15.10}$$

where the dependence on the concentration of *A* resembles the Langmuir–Hinshelwood expression and the function of the rate of photon absorption is able to describe the generally accepted dependence of the photocatalytic reaction rates: linearly with the incident light flux under low-radiation power conditions whereas the exponent decreases to 0.5 under moderate- to high-radiation power conditions.[10] This expression is compatible with the unavoidable radiation profiles present in photocatalytic reactors that make for an expected progressive change in the dependence of the reaction rate with the radiation intensity from values close to 0.5 near the photoreactor irradiated surface to 1.0 in the darker regions. This methodology has been successfully validated in several cases, such as the mineralization of 4-chlorophenol,[11] the oxidation of cyanide[12] and the inactivation of bacteria.[13]

The kinetic parameters of the proposed kinetic expression can be estimated by means of a Levenberg–Marquardt nonlinear regression algorithm that minimizes the error between the experimental data of the reaction rate ideally obtained over a wide range of different irradiation conditions, catalyst concentrations, and reactant concentrations, and the reaction rate calculated by the model after averaging the values of the reaction rate calculated in any position of the reactor with the LVRPA and concentration of reactants. Therefore, this step requires the preliminary estimation of the radiation field in the laboratory reactor and the resolution of the mass balance in the system, as schematized in Figure 15.1.

15.6 Mass Balance Equations

Once the kinetic model is available for calculating the reaction rate in every position of the reactor volume, $r_A(\underline{x},t)$, it can be used to solve the mass balance of the system. Depending on the type of photocatalytic reactor it will take a different form:

(a) the very simple expression of a well-mixed discontinuous reactor without mass transport limitation and negligible parallel dark reactions:

$$\frac{\mathrm{d}[\mathrm{A}](t)}{\mathrm{d}t} = \left\langle r_A(\underline{x},t)\right\rangle_{V_{\text{reactor}}} \tag{15.11}$$

(b) the expression for a discontinuous reactor of differential conversion working in recirculation with a reservoir:

$$\left.\frac{\mathrm{d}[\mathrm{A}](t)}{\mathrm{d}t}\right|_{\text{tank}} = \frac{V_{\text{reactor}}}{V_{\text{total}}}\left\langle r_A(\underline{x},t)\right\rangle_{V_{\text{reactor}}} \tag{15.12}$$

(c) the more general expression of a recirculation reactor in which the mass balance of a well-mixed reservoir tank is expressed as a function of the outlet of a non-ideal reactor:

$$\left.\frac{\mathrm{d}[\mathrm{A}](t)}{\mathrm{d}t}\right|_{\text{tank}} = \frac{1}{\tau_{\text{tank}}}\left([\mathrm{A}]^{\text{reactor\_outlet}}(t) - [\mathrm{A}](t)\right) \tag{15.13}$$

and the differential mass balance of the reactor is computed to calculate the reactor outlet, for instance in cylindrical coordinates and under the assumptions of: (i) steady state, (ii) negligible thermal effects, (iii) unidirectional axial flow, (iv) azimuthal symmetry, (v) negligible axial diffusion when compared to the convective flux in that direction, (vi) incompressible flow (constant ρ) and (vii) constant diffusion coefficient, $D^0_{\text{A–water}}$:

$$v_z\frac{\partial C_A}{\partial z} = D^0_{A\,-\,\text{water}}\left[\frac{1}{r}\frac{\partial}{\partial r}\left(r\frac{\partial C_A}{\partial r}\right)\right] + r_A \tag{15.14}$$

where a fluid flow model has to be adopted to estimate the velocity field, v_z.

15.7 Case Study: Photocatalytic Oxidation of Cyanide with TiO_2/SiO_2 Materials

This section presents an example of the application of the predictive simulation methodology of photoreactors to the design of a bench-scale annular photocatalytic reactor for the oxidation of cyanide in water working with a catalytic suspension of TiO_2/SiO_2 particles. First, the optical properties of the suspension were determined. This allows the estimation of the radiation absorbed by the catalyst and therefore the calculation of the quantum efficiency of the process. The development of a suitable kinetic model based on the reaction mechanism finally allowed the scaling up of the laboratory results to a larger reactor with different geometry, radiation source and fluid dynamic regime.

15.7.1 Experimental Determination of the Optical Properties of the Materials

One of the main disadvantages of photocatalytic processes employing titanium dioxide particles is the additional cost associated with the downstream catalyst separation. To overcome this limitation significant effort has been made to develop supported titania photocatalysts on particles of larger size to facilitate the sedimentation recovery process.[14] To make predictive simulations of the performance of photocatalytic reactors based on these materials, their optical properties should be determined. Following the methodology described in Section 15.2, experimental data of transmittance, diffuse transmittance and diffuse reflectance of suspensions of increasing catalyst loading of three different materials with 20, 40 and 60 wt% of TiO_2 were recorded using a flow cell. From this information, values of the specific absorption and scattering coefficients and the phase function for each material were computed and compared with those corresponding to the silica material used as support. Full details of the primary experimental information and the numerical procedure can be found elsewhere.[2] The results of the wavelength dependence of κ_λ^* and σ_λ^* in the UV-A range are summarized in Table 15.2. As it can be seen, the silica material absorption is negligible, whereas the scattering is constant in all the studied wavelength range. Incorporation of TiO_2 onto the silica particles leads to an increase in the absorption of radiation that seems to reach a maximum for 40 wt% of TiO_2 (similar absorption is observed for the 60 wt% loaded material). In all cases, the values of κ_λ^* increase significantly for lower wavelength, in agreement with the expected absorption edge of TiO_2 semiconductor crystals. TiO_2 incorporation also increases the scattering properties of the suspension. In this case the values of σ_λ^* are quite similar in all the studied wavelength range, with only a slight decrease at the lower values of λ, at which the absorption is more pronounced. Remarkably, the values of the absorption and scattering coefficients of these TiO_2/SiO_2 materials are more than one order of magnitude lower than those

Table 15.2 Specific absorption and scattering coefficients of the selected TiO_2/SiO_2 materials as a function of the wavelength in the UV-A range[6].

	SiO_2		20% TiO_2/SiO_2		40% TiO_2/SiO_2		60% TiO_2/SiO_2	
λ (nm)	κ_λ^* (cm^2 g^{-1})	σ_λ^* (cm^2 g^{-1})	κ_λ^* (cm^2 g^{-1})	σ_λ^* (cm^2 g^{-1})	κ_λ^* (cm^2 g^{-1})	σ_λ^* (cm^2 g^{-1})	κ_λ^* (cm^2 g^{-1})	σ_λ^* (cm^2 g^{-1})
325	1.3	943	335	1226	429	1502	479	1444
335	4.9	941	269	1273	333	1577	372	1544
345	4.0	937	201	1315	258	1616	290	1595
355	2.3	939	129	1369	179	1669	206	1665
365	0.8	933	58.6	1420	95.8	1722	122	1727
375	3.3	935	20.3	1441	42.7	1757	55.5	1777
385	0	929	5.9	1448	17.4	1770	24.9	1790
395	0	939	0.7	1450	7.6	1772	16.7	1790

corresponding to typical TiO_2 powders.[15] This fact has a strong impact on the optical design of the reactor, as it allows thicker optical paths.

15.7.2 Estimation of the Quantum Efficiency

Determination of the quantum efficiency of the cyanide photocatalytic oxidation process using the TiO_2/SiO_2 catalysts requires the calculation of the radiation absorption in the reactor in which the experimental reaction rates have been obtained. To make it easier, the reactor should be designed in such a way that typical assumptions that simplify the mass balance and the radiation model apply. As an example, the experimental setup shown in Figure 15.6 has the following characteristics related to the radiation transport phenomena:

(i) The high power halogen lamp allows working under high irradiation power.
(ii) The neutral filters allow regulation of the inlet radiation flux to obtain experimental data under different irradiation values.
(iii) The water filter removes all the infrared radiation to keep the temperature constant.
(iv) The irradiated window of the reactor has a ground glass texture to allow the assumption of a diffuse incoming radiation in the boundary condition of the radiation transport equation applied to the photoreactor.
(v) The whole system is covered by a black enveloped to avoid uncontrolled radiation entering the reactor.
(vi) Stirring in the reservoir tank keeps the aggregates size distribution of the particles unaltered, allowing the assumption that the optical properties of the suspension are constant along the reaction.
(vii) Absorption in the UV-A range of the chemical species dissolved in the water (not only reactants but also degradation intermediates) is negligible.

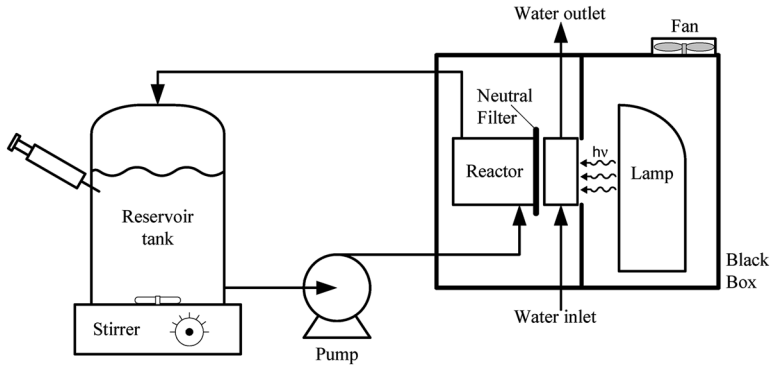

Figure 15.6 Experimental setup used for the determination of quantum efficiencies and kinetic parameters at laboratory scale. (Reprinted from ref. 4. Copyright 2007, with permission from Elsevier.)

Table 15.3 Calculated values for the average volumetric rates of photon absorption, cyanide photo-oxidation rate and quantum efficiencies for 40 wt% TiO_2/SiO_2 photocatalyst[4].

C_{cat} (g L^{-1})	$C_{CN}{}^0$ (mg L^{-1})	$q^0 \times 10^4$ (Einstein m^{-2} s^{-1})	$\langle e^a \rangle_{V_R} \times 10^3$ (Einstein m^{-3} s^{-1})	$\langle r^0_{CN} \rangle_{V_R} \times 10^5$ (mol_{CN} m^{-3} s^{-1})	η_{CN} (%)
1.0	15.0	5.86	2.02	6.86	3.4
3.0	15.0	5.86	3.39	13.3	3.9
1.0	45.0	5.86	2.02	11.4	5.6
3.0	45.0	5.86	3.39	15.3	4.5
1.0	15.0	20.0	6.91	16.1	2.3
3.0	15.0	20.0	11.6	21.0	1.8
1.0	45.0	20.0	6.91	21.3	3.1
3.0	45.0	20.0	11.6	28.8	2.5
2.0	30.0	12.9	6.48	19.5 ± 1.7	3.0 ± 0.3

Under these conditions, the radiation field in the reactor can be rigorously calculated once the boundary condition of the incident radiation is experimentally measured by actinometric or radiometric procedures, or estimated from the lamp emission model. Once known, the distribution of radiation along the photoreactor, the incident radiation and local volumetric rate of photon absorption at any position of the reactor can be determined. These values, once integrated on the wavelength range overlapping the lamp emission and the catalyst absorption, can be used to compute the volume-averaged rate of photon absorption in the photoreactor. Full details of the calculations can be found elsewhere,[4] Table 15.3 shows the results of $\langle e^a \rangle_{V_R}$ obtained for the 40 wt% TiO_2/SiO_2 material under different experimental conditions.

Regarding the mass balance of the system, there also some important features of the experimental setup to be considered:

(i) The photoreactor works in recirculation with a reservoir tank of much higher volume and under flow rates high enough to assume differential conversion per pass.
(ii) The flow regime in the reactor is close to well-mixed conditions, allowing diffusional limitations to be neglected and the assumption of kinetic control of the global reaction.
(iii) The reservoir tank is aerated to ensure a constant concentration of O_2 in water corresponding to saturation at the working temperature.
(iv) Withdrawal of samples from the reservoir tank gives the evolution the concentration of the reactant *versus* irradiation time.
(v) The accumulated volume of samples is negligible in comparison with the total liquid volume, allowing the assumption of constant volume along the reaction.
(vi) The disappearance of cyanide by adsorption and/or dark reactions can be neglected on the basis of blank experiments without illumination.

Under these conditions, the mass balance of the recirculation reactor can be expressed as follows:

$$\varepsilon_L \left.\frac{dC_{CN}(t)}{dt}\right|_{Tk} = -\frac{V_R}{V_T}\left\langle r_{CN}(x,t)\right\rangle_{V_R} \tag{15.15}$$

where ε_L is the liquid hold-up ($\varepsilon_L = 1$ for a pseudo-homogeneous system); C_{CN} is the molar concentration of cyanide; t denotes the reaction time; Tk, R and T sub-indexes refer to the tank, reactor and total, respectively; and $\langle r_{CN}(x,t)\rangle_{V_R}$ is the cyanide disappearance reaction rate averaged over the reactor volume.

Therefore, the initial reaction rate of cyanide photo-oxidation can be derived from the slope of the plot of the cyanide concentration in the tank *versus* time according to:

$$\left\langle r_{CN}^0 \right\rangle_{V_R} = -\frac{V_T}{V_R}\lim_{t\to 0}\left.\frac{dC_{CN}(t)}{dt}\right|_{Tk} \tag{15.16}$$

Table 15.3 summarizes the results obtained for the cyanide photo-oxidation rates together with the quantum efficiencies, calculated according to:

$$\eta_{CN} = \frac{\left\langle r_{CN}^0 \right\rangle_{V_R}}{\left\langle e^a \right\rangle_{V_R}} \tag{15.17}$$

As it can be noticed, the quantum efficiencies vary significantly as a function not only of the irradiation power and catalysts concentration but also depend on the cyanide concentration in solution. This effect is produced

by the kinetics of the reaction, because, for the same radiation absorption rate, the higher the cyanide concentration the higher the experimental reaction rate.

15.7.3 Development of a Suitable Intrinsic Kinetic Model

The values of the quantum efficiencies of the photocatalytic process are very helpful for optimizing the use of light, but they cannot be directly used for simulation of a different reactor. For this aim, a reaction mechanism including the radiation absorption step should be postulated and the corresponding kinetic expression derived. Table 15.4 shows the proposed reaction scheme for the cyanide photocatalytic degradation.

The following assumptions are also made:

(i) kinetic micro steady state approximation (MSSA) for the concentration of electrons, holes, hydroperoxyl radicals ($HO_2^{\bullet}$), superoxide ion radicals ($O_2^{-\bullet}$), surface trapped holes ($\equiv TiO^{\bullet}$), radical $CN^{\bullet}$ and unstable species $(CN)_2$;
(ii) concentration of electrons and holes are approximately equal ($[e^-] \approx [h^+]$);[8]
(iii) cyanide is mainly oxidized by the surface trapped holes ($k_9[h^+][CN^-] \approx 0$);[16]
(iv) the rate of electron–hole generation is proportional to the local volumetric rate of photon absorption (e^a);[17]
(v) the concentrations of water and hydroxyl ions on the catalytic surface are almost constant;
(vi) competitive adsorption of cyanide and the main intermediate products;
(vii) non-competitive adsorption of oxygen on the catalyst surface sites.[8]

Table 15.4 Reaction scheme for cyanide photocatalytic degradation. (Reprinted from ref. 12. Copyright 2008, with permission from Elsevier.).

Reaction step	Step number
$TiO_2 + h\nu \rightarrow TiO_2 + e^- + h^+$	1
$e^- + h^+ \rightarrow$ heat	2
$e^- + O_2 \rightarrow {}^{\bullet}O_2^-$	3
${}^{\bullet}O_2^- + H_2O \rightarrow HO_2^{\bullet} + HO^-$	4
$HO_2^{\bullet} + e^- \rightarrow HO_2^-$	5
$\equiv TiO^- + h^+ \rightarrow \equiv TiO^{\bullet}$	6
$HO^- + h^+ \rightarrow HO^{\bullet}$	7
$HO^- + \equiv TiO^{\bullet} \rightarrow HO^{\bullet} + \equiv TiO^-$	8
$CN^- + h^+ \rightarrow CN^{\bullet}$	9
$CN^- + \equiv TiO^{\bullet} \rightarrow CN^{\bullet} + \equiv TiO^-$	10
$\equiv TiO^{\bullet} + e^- \rightarrow \equiv TiO^-$	11
$2CN^{\bullet} \rightarrow (CN)_2$	12
$(CN)_2 + 2HO^- \rightarrow CNO^- + CN^- + H_2O$	13
$2HO^{\bullet} \rightarrow H_2O_2$	14
$2H_2O_2 \rightarrow 2H_2O + O_2$	15

On the basis of the reaction scheme in Table 15.4 and the above assumptions, the following kinetic expression is derived:[12]

$$r_{CN} = -S_g C_{cat} \frac{\alpha_1 C_{CN}}{1 + \alpha_3 C_{CN} + \sum_P K_P [P_b]} \left[-1 + \sqrt{1 + \frac{\alpha_2}{S_g C_{cat}} e^a} \right] \qquad (15.18)$$

where r_{CN} is the cyanide photocatalytic degradation rate per unit suspension volume, C_{CN} is the cyanide molar concentration in the suspension bulk, e^a is the LVRPA, S_g is the catalyst specific surface area, C_{cat} is the catalyst mass concentration, and α_1, α_2, and α_3 are kinetic parameters.

Assuming a negligible concentration of intermediate products (initial reaction rate calculations), estimation of the reaction rate of the photocatalytic oxidation of cyanide just requires the values of the catalysts concentration, cyanide concentration and photon absorption rate averaged in the reactor volume according to:

$$\left\langle r^0_{CN} \right\rangle^{KM}_{V_R} = -S_g C_{cat} \frac{\alpha_1 C_{CN}}{1 + \alpha_3 C_{CN}} \left(-1 + \left\langle \sqrt{1 + \frac{\alpha_2 e^a}{S_g C_{cat}}} \right\rangle_{V_R} \right) \qquad (15.19)$$

Estimation of the kinetic parameters α_1, α_2, and α_3 was carried out using a Levenberg–Marquardt nonlinear regression algorithm by comparison of the $\left\langle r^0_{CN} \right\rangle^{KM}_{V_R}$ values with the corresponding experimental data, leading to:

$$\begin{aligned} \alpha_1 &= 9.94 \pm 0.14 \times 10^{-7}\ \text{cm s}^{-1} \\ \alpha_2 &= 1.99 \pm 0.05 \times 10^{11}\ \text{cm}^2\ \text{s Einstein}^{-1} \\ \alpha_3 &= 5.27 \pm 0.16 \times 10^{5}\ \text{cm}^3\text{mol}^{-1} \end{aligned} \qquad (15.20)$$

for the 40 wt% TiO_2/SiO_2 material ($S_g = 19.3 \times 10^4\ \text{cm}^2\ \text{g}^{-1}$, corresponding only to the active semiconductor surface estimated using a previously reported method[18]).

15.7.4 Scaling-Up of the Process to a Larger Photocatalytic Reactor

The predictive simulation of a larger photocatalytic reactor can be addressed once the intrinsic kinetic model of the process has been determined. The designed bench-scale photoreactor has an irradiated volume ten times higher, an annular geometry and a tubular black light fluorescent lamp, in contrast with the metal halide lamp used in the laboratory photoreactor (Figure 15.7). Being rigorous the intrinsic kinetic model should be applied only to other reactor configurations using light sources with a similar spectral distribution of the emitted radiation, because the kinetic parameter α_2 defined during the derivation of the kinetic model includes the value of the

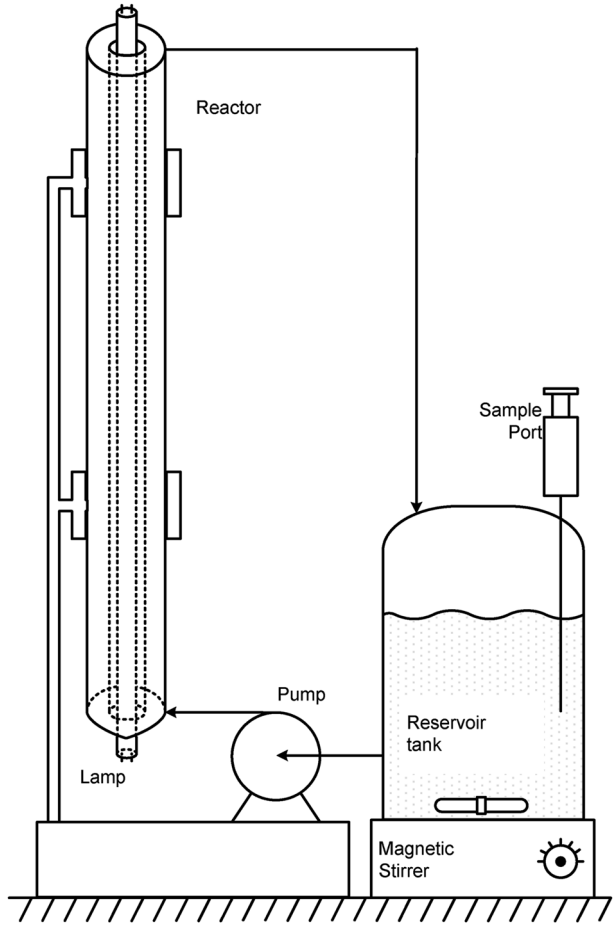

Figure 15.7 Schematic representation of the bench-scale photoreactor. (Reprinted from ref. 19. Copyright 2009, with permission from Elsevier.)

wavelength averaged primary quantum yield.[12] In this case, although both lamp types are not exactly the same, the emission spectra could be considered to be quite similar, and it was assumed that the values of the kinetic parameters shown in eqn (15.20) are valid for the bench scale system.

The radiation field in the photoreactor was calculated by solving the RTE using a two-dimensional, two-directional radiation model and a numerical procedure based on the discrete ordinate method (see Chapter 14) similar to that of the laboratory-scale photoreactor (detailed elsewhere[12]). From the intensity of radiation data, the values of the local volumetric rate of photon absorption were estimated.[19] However, in this case the well-mixed condition cannot be applied to the photoreactor, and consequently the differential form of the mass conservation equation must be used. Under the following

assumptions: (i) steady state, (ii) negligible thermal effects, (iii) unidirectional axial flow, (iv) azimuthal symmetry, (v) negligible axial diffusion when compared to the convective flux in that direction, (vi) incompressible flow (constant ρ) and (vii) constant diffusion coefficient ($D^0_{CN^-\text{–water}} = 1.25 \pm 0.05 \times 10^{-5}$ cm^2 s^{-1} (ref. 20)), the mass balance in cylindrical coordinates can be expressed as follows:

$$v_z(r)\frac{\partial C_{CN}(z,r)}{\partial z} = D^0_{CN^-\text{–water}}\left[\frac{1}{r}\frac{\partial}{\partial r}\left(r\frac{\partial C_{CN}(z,r)}{\partial r}\right)\right] + r_{CN}(z,r) \tag{15.21}$$

with the following boundary conditions:

$$C_{CN}(z=0,r) = C_{CN}(t)$$
$$\frac{\partial C_{CN}(z,r_{int})}{\partial r} = \frac{\partial C_{CN}(z,r_{ext})}{\partial r} = 0 \tag{15.22}$$

The resolution of the mass conservation eqn (15.21) was carried out using a Crank–Nicholson finite differences scheme, assuming a parabolic profile for the radial velocity distribution in the annular space. The solution provides the cyanide concentration profiles along the reactor, making possible the estimation of the reactor outlet concentration required for resolution of the mass balance in the recirculation system:

$$\left.\frac{dC_{CN}(t)}{dt}\right|_{Tk} = \frac{1}{\tau_{Tk}}\left(C^{inlet}_{CN}(t) - C_{CN}(t)\right) \tag{15.23}$$

that can be solved with the initial condition:

$$C_{CN}(t=0) = C^0_{CN} \tag{15.24}$$

using a conventional Runge–Kutta numerical method. The value of the inlet cyanide concentration in the tank is calculated from the outlet concentration of the reactor.

Figure 15.8 shows a comparison between the predictions of the simulation model and the experimental results obtained in the constructed bench-scale photoreactor for different catalysts and cyanide concentrations using the 40 wt% TiO_2/SiO_2 photocatalyst. A very good agreement is observed, with a normalized root mean square error of 6.2%. Importantly, the lines in the plot do not correspond to a fitting of the experimental data but to a full predictive simulation of the reactor operations based on the kinetic laboratory-scale data obtained in a different reaction system.

In conclusion, this example validates the procedure of photoreactor simulation based on the determination of the intrinsic kinetics of the reaction at laboratory scale. Based on this information, the model of a larger scale reactor has predicted with good accuracy its experimental performance, validating the applicability of the whole methodology for photocatalytic reactor design.

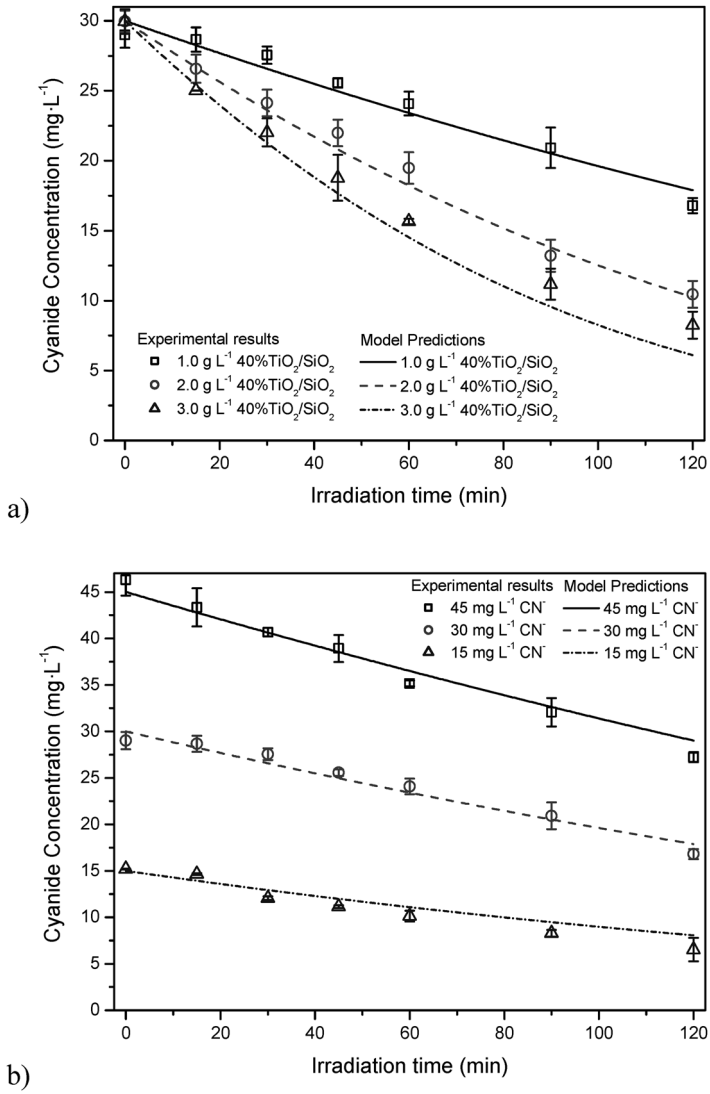

Figure 15.8 Experimental results and model predictions of the operation of the bench-scale reactor with 40 wt% TiO_2/SiO_2: (a) effect of catalyst concentration at a fixed initial cyanide concentration of 30 mg L^{-1}; (b) effect of initial cyanide concentration at a fixed catalyst concentration of 1.0 g L^{-1}. (Reprinted from ref. 19. Copyright 2009, with permission from Elsevier.)

Acknowledgements

The authors gratefully acknowledge the financial support of the Spanish Ministry of Economy and Competitiveness (WATER4FOOD, CTQ2014-54563-C3-1-R) and Comunidad de Madrid (REMTAVARES, S2013/MAE-2716). In addition, they acknowledge the financial support from the Universidad

Nacional del Litoral, Agencia Nacional de Promoción Científica y Tecnológica, and Consejo Nacional de Investigaciones Científicas y Técnicas of Argentina.

References

1. M. L. Satuf, R. J. Brandi, A. E. Cassano and O. M. Alfano, *Ind. Eng. Chem. Res.*, 2005, **44**, 6643.
2. J. Marugán, R. van Grieken, O. M. Alfano and A. E. Cassano, *AIChE J.*, 2006, **52**, 2832.
3. S. E. Braslavsky, A. M. Braun, A. E. Cassano, A. V. Emeline, M. I. Litter, L. Palmisano, V. N. Parmon and N. Serpone, *Pure Appl. Chem.*, 2011, **83**, 931.
4. J. Marugán, R. van Grieken, A. E. Cassano and O. M. Alfano, *Catal. Today*, 2007, **129**, 143.
5. J. Marugán, D. Hufschmidt, G. Sagawe, V. Selzer and D. Bahnemann, *Water Res.*, 2006, **40**, 833.
6. C. Minero, *Sol. Energy Mater. Sol. Cells*, 1995, **38**, 421.
7. A. Mills, J. Wang and D. F. Ollis, *J. Catal.*, 2006, **243**, 1.
8. C. S. Turchi and D. F. Ollis, *J. Catal.*, 1990, **122**, 178.
9. O. M. Alfano, M. I. Cabrera and A. E. Cassano, *J. Catal.*, 1997, **172**, 370.
10. J. M. Herrmann, *Catal. Today*, 1999, **53**, 115.
11. M. L. Satuf, R. J. Brandi, A. E. Cassano and O. M. Alfano, *Appl. Catal., B*, 2008, **82**, 37.
12. J. Marugán, R. van Grieken, A. E. Cassano and O. M. Alfano, *Appl. Catal., B*, 2008, **85**, 48.
13. J. Marugán, R. van Grieken, C. Pablos, M. L. Satuf, O. M. Alfano and A. E. Cassano, *Appl. Catal., B*, 2011, **102**, 404.
14. J. Aguado, R. van Grieken, M. J. López-Muñoz and J. Marugán, *Catal. Today*, 2002, **75**, 95.
15. M. I. Cabrera, O. M. Alfano and A. E. Cassano, *J. Phys. Chem.*, 1996, **100**, 20043.
16. K. Chiang, R. Amal and T. Tran, *J. Mol. Catal. A: Chem.*, 2003, **193**, 285.
17. O. M. Alfano, M. I. Cabrera and A. E. Cassano, *J. Catal.*, 1997, **172**, 370.
18. J. Marugán, M. J. López-Muñoz, J. Aguado and R. van Grieken, *Catal. Today*, 2007, **124**, 103.
19. J. Marugán, R. van Grieken, A. E. Cassano and O. M. Alfano, *Catal. Today*, 2009, **144**, 87.
20. X. Sun, Y. C. Guan and K. N. Han, *Metall. Mater. Trans. B*, 1996, **27**, 355.